



Electron acceleration and formation of power-law spectra of energetic electrons during the merging process of multiple magnetic islands: particle-in-cell simulations

Yu Liu^{1,2} · Quanming Lu^{1,2} · Rongsheng Wang^{1,2} · Kai Huang^{1,2} · Huanyu Wang^{1,2} · Shui Wang^{1,2}

Received: 30 December 2018 / Accepted: 24 June 2019
© Springer Nature B.V. 2019

Abstract Magnetic reconnection is considered to be one important source to produce energetic electrons. In this paper, two-dimensional (2D) particle-in-cell (PIC) simulations are performed to investigate electron acceleration during the merging process of multiple magnetic islands in a current sheet with a strong guide field. Due to the existence of the strong guide field, we can analyze the contributions of the parallel electric field, Fermi, and betatron mechanisms to the electron acceleration with the guiding-center theory. During the coalescence process of magnetic islands, the islands merge each other continuously until only one large island remains. Energetic electrons are generated during such process, and the electrons with sufficient high energy develop a power-law spectrum. We also investigate the dependence of the index of the power-law spectra on the shape of magnetic islands, electron plasma beta, the number of magnetic islands, and the guide field.

Keywords Magnetic reconnection · Energetic electrons · Magnetic islands · Power-law spectrum

1 Introduction

Energetic electrons are closely related to physical phenomena in astrophysical and space environments, such as gamma

ray bursts (Drenkhahn and Spruit 2002), solar flares (Miller et al. 1997), substorms in Earth's magnetosphere (Imada et al. 2007), and these energetic electrons usually develop power-law spectra (Øieroset et al. 2002; Holman et al. 2003; Krucker et al. 2010; Oka et al. 2015). Magnetic reconnection is a fundamental physical process, which dissipates magnetic energy into plasma kinetic energy by changing the topology of magnetic field lines. The production of energetic electrons is also a critical signature in magnetic reconnection, and thus it may provide a possible mechanism to explain the ubiquitously observed energetic electrons in these explosive phenomena.

It is generally accepted that electrons can be accelerated by the reconnection electric field near the X line and the parallel electric field in the separatrix region (Hoshino et al. 2001; Drake et al. 2005; Fu et al. 2006; Huang et al. 2010, 2012; Wang et al. 2014). Besides, electrons can be accelerated by the betatron process in the jet front, where magnetic field is piled up by the high-speed outflow from the X line (Fu et al. 2011, 2013; Birn et al. 2013; Wu et al. 2013, 2015; Huang et al. 2014; Lu et al. 2014, 2016; Zhou et al. 2018), and also the Fermi process when they are reflected at the two ends of a contracting magnetic island (Fu et al. 2006; Drake et al. 2006a). However, how a power-law spectrum of energetic electrons is formed during magnetic reconnection is still a puzzle

Recently, magnetic islands, which can be formed in a current sheet via multiple X line reconnection (Drake et al. 2006b; Daughton et al. 2006; Wang et al. 2010; Lu et al. 2014; Ma et al. 2015; Guo et al. 2018) or induced through Kelvin-Helmholtz instability in a current sheet with a strong shear flow (Nakamura and Fujimoto 2008; Huang et al. 2017), are considered to play a critical role in electron acceleration during magnetic reconnection (Fu et al. 2006; Chen et al. 2008; Pritchett 2008; Oka et al. 2010; Li et al.

✉ Q. Lu
qmlu@ustc.edu.cn

✉ R. Wang
rswan@ustc.edu.cn

¹ CAS Key Lab of Geospace Environment, School of Earth and Space Sciences, University of Science and Technology of China, Hefei 230026, China

² CAS Center for Excellence in Comparative Planetology, Hefei, China

2017; Wang et al. 2016, 2017). With the formation of magnetic islands, electrons can be easily trapped in or around the magnetic islands, and experience multiple acceleration near the X line by the reconnection electric field or Fermi process inside the magnetic islands. Magnetic islands also tend to coalesce and form large islands (Finn and Kaw 1977; Pritchett 2007; Wang et al. 2016; Zhao et al. 2016; Zhou et al. 2017), and electrons are found to be accelerated during such a process. With two-dimensional (2-D) particle-in-cell (PIC) simulations, Lu et al. (2018) investigated the process of electron acceleration in multiple X line reconnection with a guide field, and in such a process magnetic islands are generated at first and then coalesce with each other. Electrons can be accelerated during both the generation and the coalescence of magnetic islands by the parallel electric field and Fermi mechanism, and at last form a power-law distribution. In order to know more clearly electron acceleration during the coalescence of magnetic islands, in this paper we perform 2-D PIC simulations to study the evolution of a chain of preexisting magnetic islands in a current sheet and associated electron acceleration, and the influences of the shape of magnetic islands, electron plasma beta, the number of magnetic islands, and the guide field, are also considered. Here, in the current sheet, there is a strong guide field, and electron motions can be assumed to be adiabatic. Therefore, we can analyze the electron acceleration with the help of the guiding-center theory. According to the guiding-center theory, the total electron kinetic energy is governed by the following equation (Northrop 1963; Dalin et al. 2014),

$$\frac{dU}{dt} = E_{\parallel} J_{\parallel} + \frac{p_{\perp}}{B} \left(\frac{\partial B}{\partial t} + \mathbf{u}_E \cdot \nabla B \right) + (p_{\parallel} + m_e n u_{\parallel}^2) \mathbf{u}_E \cdot \boldsymbol{\kappa} \tag{1}$$

where U is the total electron kinetic energy, B is the amplitude of the magnetic field, E_{\parallel} , J_{\parallel} and u_{\parallel} are the electric field, electron current density and electron bulk velocity parallel to the magnetic field, \mathbf{u}_E is the “ $\mathbf{E} \times \mathbf{B}$ ” drift velocity, n is the electron number density, and p_{\perp} , p_{\parallel} are the perpendicular and parallel pressures, and $\boldsymbol{\kappa} = \mathbf{b} \cdot \nabla \mathbf{b}$ (where $\mathbf{b} = \mathbf{B}/B$) is the curvature of magnetic field lines. The first term in the right hand of Eq. (1) represents the electron acceleration by the parallel electric field, and the second is the betatron mechanism. The last term is the contribution from the Fermi mechanism.

2 Simulation model

We investigate the electron acceleration during merging process of a chain of preexisting magnetic islands by carrying

out 2D PIC simulations. In the simulations, the electromagnetic fields are defined on the grids in the x - z plane and updated by solving the Maxwell equations with a full explicit algorithm. The particles can move in the x - z plane, but retains all three components of their velocities, and they are advanced by the Lorentz force. The initial configuration for the simulations is the island-chain equilibrium described by the vector potential component

$$A_y(x, z) = -\lambda B_0 \ln \left[\cosh \frac{z}{\lambda} + \varepsilon \cos \frac{x}{\lambda} \right] \tag{2}$$

where B_0 is the asymptotic magnetic field, and λ gives the half-thickness of the current sheet, ε determines the shape of magnetic island, or the relation between the width of the initial island δ and the half-thickness of the current sheet λ , which is $\delta/\lambda = \cosh^{-1}(1 + 2\varepsilon)$ (where $0 \leq \varepsilon < 1$). The magnetic field can be determined in the following way: $B_x = -\partial A_y/\partial z$, $B_z = \partial A_y/\partial x$, and $B_y = B_{0y}$ is the guide field. The corresponding number density n can be described as

$$n(x, z) = n_b + n_0 \frac{1 - \varepsilon^2}{(\cosh \frac{z}{\lambda} + \varepsilon \cos \frac{x}{\lambda})^2} \tag{3}$$

where n_b is the number density of the background plasma, and n_0 gives the number density in the center of the current sheet. The initial distribution functions for ions and electrons are Maxwellian with a drift velocity in the y direction, and their drift speeds satisfy $V_{i0}/V_{e0} = -T_{i0}/T_{e0}$, where $V_{i0}(V_{e0})$ and $T_{i0}(T_{e0})$ are the drift speed and initial temperature for ions(electrons), respectively. In our simulations, we set $n_0 = 5n_b$, the mass ratio of ion to electron $m_i/m_e = 100$ and the light speed $c = 15V_A$ (where V_A is the Alfvén speed defined by B_0 and n_0). The computations are carried out in a rectangular domain with the dimension $L_x \times L_z = 60d_i \times 15d_i$, where $d_i = c/\omega_{pi}$ is the ion inertial length defined by n_0 . The grid number is $N_x \times N_z = 1200 \times 300$, so the spatial resolution is $\Delta x = \Delta z = 0.05d_i$. The maximum of Δx over λ_d ($(\Delta x/\lambda_d)_{\max}$, λ_d is the Debye length based on n_0 , T_{i0} and T_{e0}) is about 1.2 among all the simulations. The time step is $\Omega_i \Delta t = 0.001$, where $\Omega_i = eB_0/m_i$ is the ion gyro-frequency based on B_0 . We employ more than 10^8 particles per species in the simulations. The periodic boundary conditions are used in the x direction, while the ideal conducting boundary conditions for electromagnetic fields and reflected boundary conditions for particles are employed in the z direction.

3 Simulation results

In this paper, we investigate the coalescence process of magnetic islands and associated electron acceleration by

Table 1 Parameters for the various simulation runs

Run	B_{0y}/B_0	N	β_e	ε	p^a	$\Omega_i T^b$
1	1.0	10	0.2	0.50	2.09	215
2	1.0	10	0.2	0.25	2.49	355
3	1.0	10	0.2	0.65	2.61	165
4	1.0	10	0.3	0.50	1.93	215
5	1.0	10	0.4	0.50	2.23	215
6	1.0	7	0.2	0.50	1.91	255
7	1.0	20	0.2	0.50	2.66	140
8	1.5	10	0.2	0.50	2.31	245
9	2.0	10	0.2	0.50	2.59	300

^a p is the index of the power-law spectrum of energetic electrons

^b T is the total time for the system from the beginning to the end of the merging process (when only one large island remains)

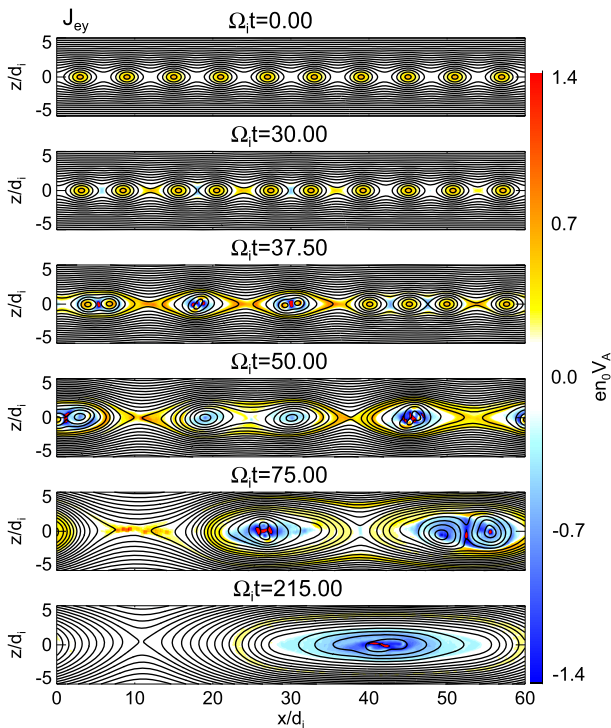


Fig. 1 Magnetic field lines in the x - z plane and the electron current in the y direction (J_{ey}) at $\Omega_i t = 0, 30, 37.5, 50, 75, 215$ for Run 1.

changing the following parameters: ε , the electron plasma beta $\beta_e = 2\mu_0 n_0 T_{e0}/B_0^2$, the number of magnetic islands in the simulation domain N (N is controlled by changing the length of the magnetic island l ($l = 2\pi/(1/\lambda) = 2\pi\lambda$) through the relation $N = L_x/l$), and the guide field B_{0y} . The details of all runs are listed in Table 1.

Figure 1 shows the evolution of the electron current in the y direction (J_{ey}) during the coalescence process of magnetic islands for Run 1. The initial configuration is an island-chain with ten magnetic islands, and the electron current pointing to the y direction (J_{ey}) is mainly located within the magnetic islands. At about $\Omega_i t = 30$, the magnetic islands at $x \approx 15d_i$ and $x \approx 21d_i$ get closer to each other and begin to merge at $x \approx 18d_i$. At about $\Omega_i t = 37.5$, the two islands co-

alesce into one large island, which takes about only $7.5\Omega_i^{-1}$. At the same time, an elongated current sheet is generated at $x \approx 12d_i$, whose current directs to the y direction, which is opposite to the current around the merging point at $x \approx 18d_i$. The islands continue to merge each other, and there are only five magnetic islands remain at about $\Omega_i t = 50$, and this process only takes about $12.5\Omega_i^{-1}$. At about $\Omega_i t = 75$, there are three large magnetic islands and the merging process is completed at about $\Omega_i t = 215$ when only one large island remains.

In our simulations, a strong guide field is used, and the electron motions can be considered to adiabatic, and the evolution of electron kinetic energy can be governed by Eq. (1). In Fig. 2, from the left to the right panel, we plot the spatial distribution of the contributions from the parallel electric field, Fermi, and betatron mechanisms to the electron kinetic energy for Run 1 at $\Omega_i t =$ (a) 30, (b) 37.5, (c) 50, and (d) 75, respectively. When the merging process just begins, the contributions of these three mechanisms are weak. As the merging proceeds, we can see stronger contributions from the parallel electric field and Fermi mechanisms. The contribution of the parallel electric field mechanism is mainly distributed in the vicinity of X lines and the merging points, while that from the Fermi mechanism is concentrated at the two ends of the contracting magnetic islands. The contribution from the betatron mechanism remains small and is negligible during the whole merging process. This can be demonstrated more clearly in Fig. 3, which plots the contributions from the parallel electric field, Fermi, and betatron mechanisms to the evolution of electron kinetic energy for Run 1 after they are integrated in the whole simulation domain. The contributions are important during $\Omega_i t = 30$ – 120 . Notice that after this time period, there are only two large magnetic islands in the simulation domain, and the merging process of these two large magnetic islands is very slow, which leads to the slow increase of electron kinetic energy. We can also find that the contribution from the parallel electric field is larger than that from the Fermi mechanism.

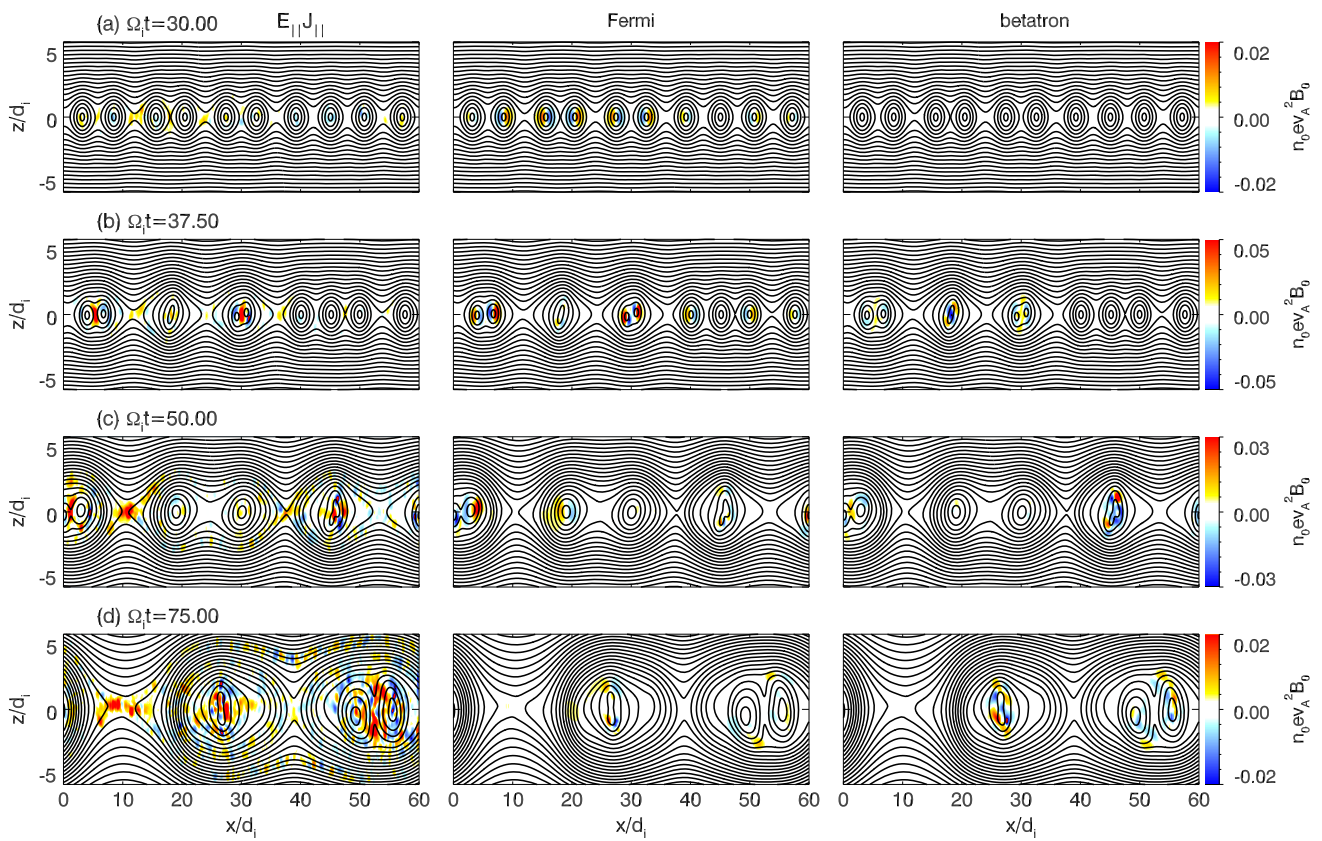


Fig. 2 From the left to the right, the panels above depict the spatial distribution of the contributions of the parallel electric field, Fermi, and betatron mechanisms to the electron acceleration at $\Omega_i t =$ (a) 30, (b) 37.5, (c) 50, (d) 75 for Run 1.

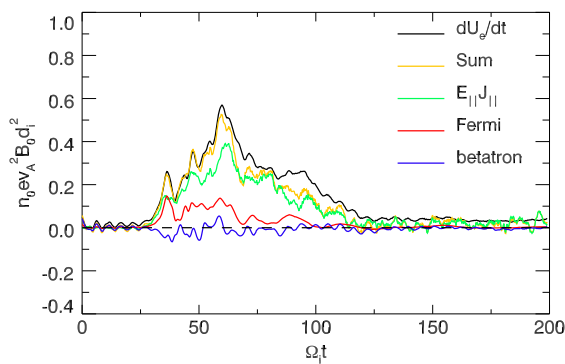


Fig. 3 The contributions of the parallel electric field, Fermi, and betatron mechanisms to the electron acceleration in the whole simulation domain for Run 1. The “Sum” is the sum of the parallel electric field, Fermi, and betatron mechanisms, and dU_e/dt represents the total electron kinetic energy change.

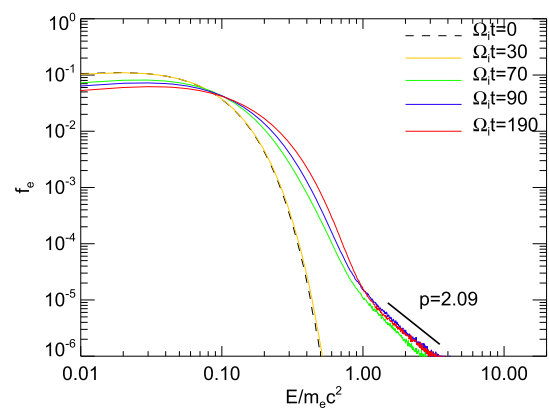


Fig. 4 The electron energy spectra at $\Omega_i t = 0, 30, 70, 90, 190$ for Run 1. The black dashed line is the initial electron energy spectrum, which is a Maxwellian distribution, and the black solid line is the fitted power-law distribution at high electron energy at the time $\Omega_i t = 190$ with an index $p = 2.09$.

Figure 4 shows the electron energy spectra for Run 1 at $\Omega_i t = 0, 30, 70, 90$ and 190. Initially, the distribution of the electrons displays a Maxwellian function. As the merging process goes on, there forms a non-thermal tail. At about $\Omega_i t = 70$, a power-law spectrum for energetic electrons is formed. The index of the power-law spectrum al-

most doesn't change after $\Omega_i t = 90$, which is estimated to be 2.09 at $\Omega_i t = 190$.

We further investigate the influence of the parameter ε on the evolution of magnetic island coalescence. In general, with the increase of the parameter ε , the initial magnetic is-

lands become round, and process of island coalescence becomes faster, for the initial width of the current sheet between each two islands is thinner, causing the earlier start-up of the merging process. This can be seen more clearly in Fig. 5, which shows the evolution of the electron current in the y direction (J_{ey}) during the coalescence process of magnetic islands for Run 3. The merging process is completed at about $\Omega_i t = 165$. Figure 6 describes the contributions from the parallel electric field, Fermi, and betatron mechanisms

to the evolution of electron kinetic energy after they are integrated in the whole simulation domain, and the electron energy spectra at $\Omega_i t = 170$ for (a) Run 2 and at $\Omega_i t = 130$ for (b) Run 3. With the increase of the parameter ε , the total electron energy gain calculated by integrating $dU_e dt$ over time increases, for there is more free magnetic energy with a larger ε . There forms a power-law spectrum for both runs, and the indexes are 2.49 and 2.61 for Run 2 and 3, respectively.

Figure 7 shows the contributions from the parallel electric field, Fermi and betatron mechanisms to the evolution of electron kinetic energy after they are integrated in the whole simulation domain and the electron energy spectra at $\Omega_i t = 190$ for (a) Run 4 and (b) Run 5. The change of the electron plasma β_e almost doesn't change the process of magnetic island coalescence, and these contributions mainly occur during the time period $\Omega_i t = 30-120$. We can also find that with the increase of the electron plasma β_e , although the contribution of the Fermi mechanism becomes larger, the total electron energy gain calculated by integrating $dU_e dt$ is nearly the same. The indexes of the power-law spectra are 1.93 and 2.23 for Run 4 and 5, respectively.

The evolution of the island coalescence has also been investigated by changing the number of magnetic islands in the simulation domain, and the increase of the number of magnetic islands will expedite the coalescence process. Figure 8 shows the evolution of the electron current in the y direction (J_{ey}) during the coalescence process of magnetic islands for Run 7. Initially, there are twenty magnetic islands in the simulation domain. We can see that the merging process is much faster compared with Run 1, where initially there are ten islands. At about $\Omega_i t = 37.5$, there are only four magnetic islands in the simulation domain. These magnetic islands finally merge into one large island at about

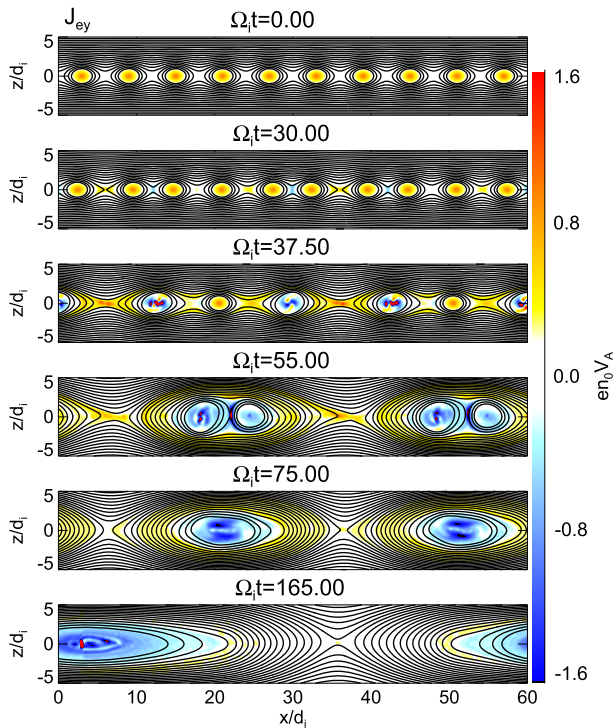
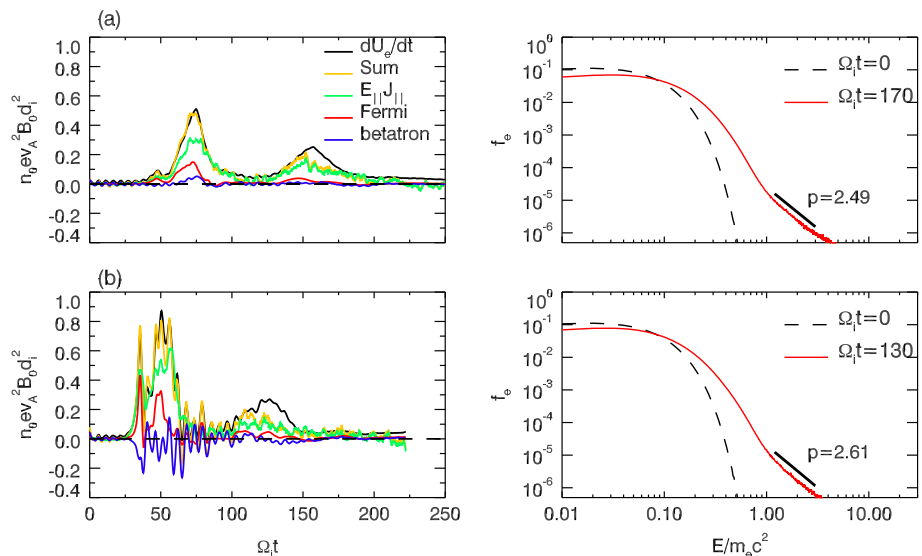


Fig. 5 Magnetic field lines in the $x-z$ plane and the electron current in the y direction (J_{ey}) at $\Omega_i t = 0, 30, 37.5, 55, 75, 165$ for Run 3.

Fig. 6 Plots of the contributions of the parallel electric field, Fermi, and betatron mechanisms in the whole simulation domain and the electron energy spectra at $\Omega_i t = 170$ for (a) Run 2 and at $\Omega_i t = 130$ for (b) Run 3, respectively.



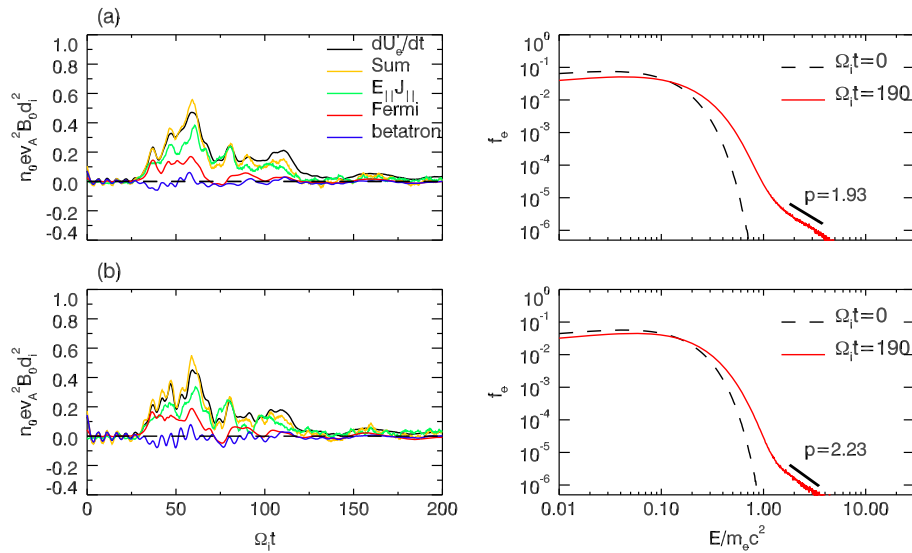


Fig. 7 Plots of the contributions of the parallel electric field, Fermi, and betatron mechanisms in the whole simulation domain and the electron energy spectra at $\Omega_i t = 190$ for (a) Run 4 and (b) Run 5, respectively.

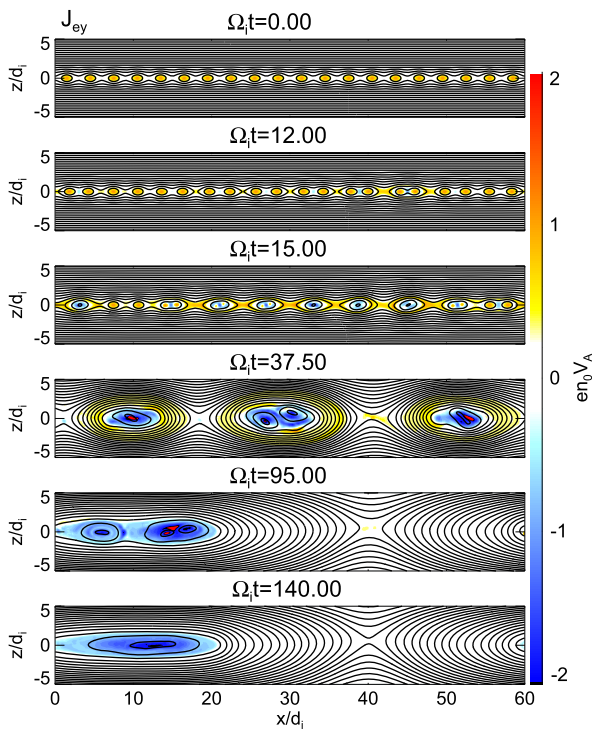


Fig. 8 Magnetic field lines in the $x-z$ plane and the electron current in the y direction (J_{ey}) at $\Omega_i t = 0, 12, 15, 37.5, 95, 140$ for Run 7.

$\Omega_i t = 140$. Figure 9 shows the contributions of the parallel electric field, Fermi, and betatron mechanisms to the evolution of electron kinetic energy after they are integrated in the whole simulation domain, and the electron energy spectra at $\Omega_i t = 200$ for (a) Run 6 and at $\Omega_i t = 170$ for (b) Run 7, respectively. With the increase of the initial num-

ber of magnetic islands, the coalescence process becomes faster, and the total electron energy gain calculated by integrating $dU_e dt$ over time increases. This is also because that there is more free magnetic energy when there are more magnetic islands. The indexes of the power-law spectra for the suprathermal electron in Run 6 and 7 are 1.91 and 2.66, respectively.

Figure 10 shows the evolution of the electron current in the y direction (J_{ey}) during the coalescence process of magnetic islands for Run 9. Compared with Run 1, now the merging process of magnetic islands is slower. The merging process is completed at about $\Omega_i t = 300$. Figure 11 plots the contributions of the parallel electric field, Fermi, and betatron mechanisms to the evolution of electron kinetic energy after they are integrated in the whole simulation domain, and the electron energy spectra at $\Omega_i t = 280$ for (a) Run 8 and (b) Run 9. Obviously, with the increase of guide field, the contribution of Fermi mechanism becomes less important, which is in accordance with the previous study (Wang et al. 2016; Lu et al. 2018). The power-law index of the suprathermal electrons also increases with the increase of guide field, which are about 2.31 and 2.59 for Run 8 and 9, respectively.

4 Summary and discussion

In this paper, we study the coalescence of magnetic islands and the produced suprathermal electrons by employing a 2D PIC simulation model. In order to analyze the contributions of the parallel electric field, Fermi and betatron mechanisms to the production of suprathermal electrons based on the

Fig. 9 Plots of the contributions of the parallel electric field, Fermi, and betatron mechanisms in the whole simulation domain and the electron energy spectra at $\Omega_i t = 200$ for (a) Run 6 and at $\Omega_i t = 170$ for (b) Run 7, respectively.

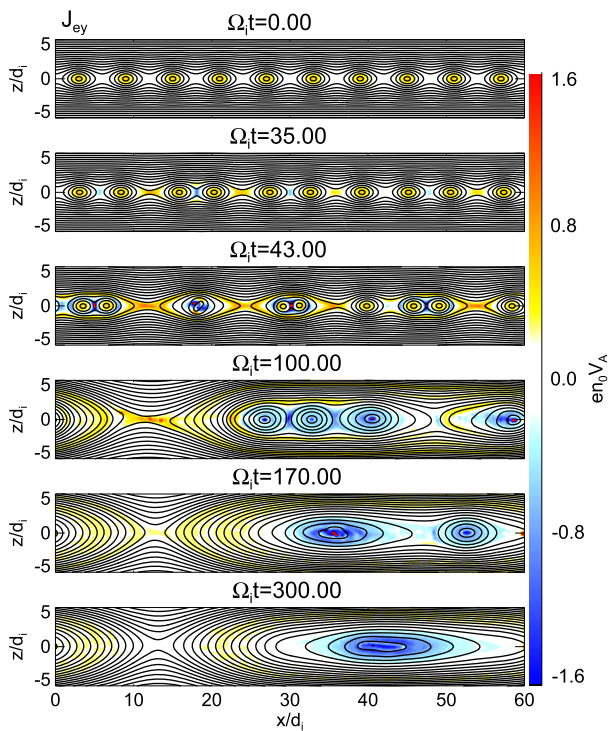
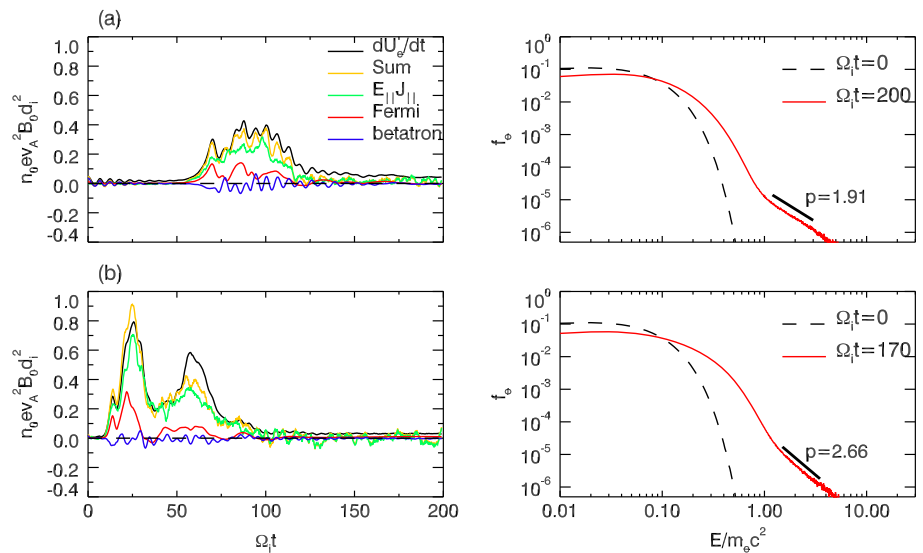


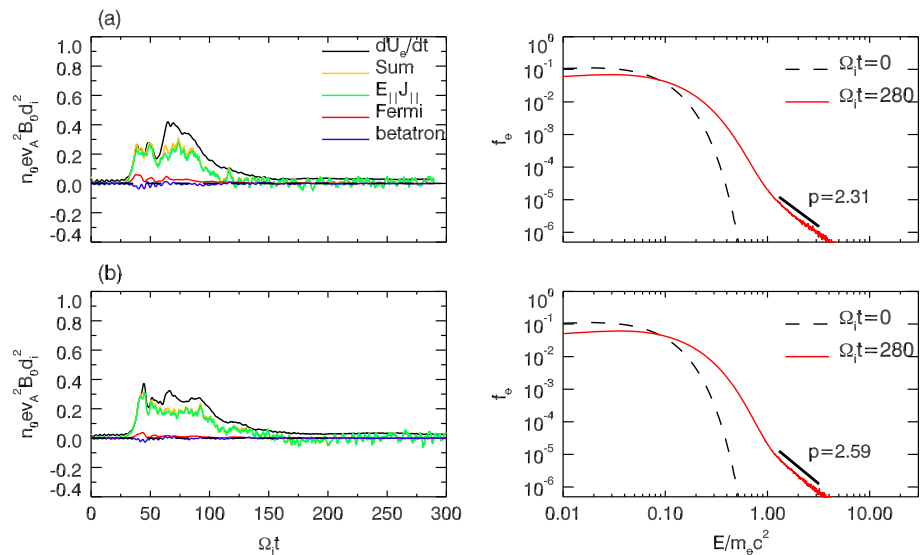
Fig. 10 Magnetic field lines in the $x-z$ plane and the electron current in the y direction (J_{ey}) at $\Omega_i t = 0, 35, 43, 100, 170, 300$ for Run 9.

guiding-center theory, a strong guide field is used in our simulations. We can find that these magnetic islands will merge each other, and at last one large island remains. At the same time, suprathermal electrons, which have a power-law spectrum when the energy is sufficiently high, are produced during the coalescence process of magnetic islands. These suprathermal electrons are accelerated mainly by the parallel electric field and Fermi mechanism. The parameters,

including ε , the electron plasma beta β_e , the initial number of magnetic islands in the simulation domain and the guide field B_{0y} can significantly influence the resulted power-law spectra formed during the coalescence process of magnetic islands. The increase of the number of magnetic islands and the guide field can result in the increase of the index of power-law spectrum in our simulations.

The energetic electrons observed in astrophysical and space environments usually have a power-law spectrum, and magnetic reconnection is considered to be one possible source to produce power-law distribution of energetic electrons (Guo et al. 2014; Li et al. 2017; Lu et al. 2018). Drake et al. (2013) and Zank et al. (2014) investigate the formation of power spectrum of energetic electrons during the interactions of islands, and give an analytical results, and the essence is that the electrons with higher energy will get a more higher acceleration efficiency. In this paper, we find that a power-law distribution of energetic electrons is easy to be formed during the coalescence of magnetic islands. Magnetic islands are easy to be generated during magnetic reconnection. For example, Shibata et al. (1995) proposed a plasmoid-induced-reconnection model to explain the plasmoids ejected during solar flares, where small scale magnetic islands (plasmoids) created by small scale tearing will be ejected and collide each other to produce larger islands by coalescence, and at last a large scale island will be ejected (Shibata and Tanuma 2001, Shibata and Takasao 2016). Therefore, our simulations provides a potential way to explain power-law spectra of energetic electrons ubiquitously observed in explosive phenomena in astrophysical and space environments.

Fig. 11 Plots of the contributions of the parallel electric field, Fermi, and betatron mechanisms in the whole simulation domain and the electron energy spectra at $\Omega_i t = 280$ for (a) Run 8 and (b) Run 9, respectively.



Acknowledgements This work was supported by the NSFC grant 41527804, 41774169, and Key Research Program of Frontier Sciences, CAS(QYZDJ-SSW-DQC010). Simulations were performed on TH-1A at National Super-Computer Center in Tianjin.

Publisher's Note Springer Nature remains neutral with regard to jurisdictional claims in published maps and institutional affiliations.

References

- Birn, J., Hesse, M., Nakamura, R., Zaharia, S.: *J. Geophys. Res.* **118**, 1960 (2013)
- Chen, L.J., Bhattacharjee, A., Puhl-Quinn, P.A., Yang, H., Bessho, N., Imada, S., Mühlbacher, S., Daly, P.W., Lefebvre, B., Khotyaintsev, Y., Vaivads, A., Fazakerley, A., Georgescu, E.: *Nat. Phys.* **4**, 19 (2008)
- Dalin, J.T., Drake, J.F., Swisdak, M.: *Phys. Plasmas* **21**, 092304 (2014)
- Daughton, W., Scudder, J., Karimabadi, H.: *Phys. Plasmas* **13**, 072101 (2006)
- Drake, J.F., Shay, M.A., Thongthai, W., Swisdak, M.: *Phys. Rev. Lett.* **94**, 095001 (2005)
- Drake, J.F., Swisdak, M., Che, H., Shay, M.A.: *Nature* **443**, 553 (2006a)
- Drake, J.F., Swisdak, M., Schoeffler, K.M., Rogers, B.N., Kobayashi, S.: *Geophys. Res. Lett.* **33**, L13105 (2006b)
- Drake, J.F., Swisdak, M., Fermo, R.: *Astrophys. J. Lett.* **763**, L5 (2013)
- Drenkhahn, G., Spruit, H.C.: *Astron. Astrophys.* **391**, 1141 (2002)
- Finn, J.M., Kaw, P.K.: *Phys. Fluids* **20**, 72 (1977)
- Fu, X.R., Lu, Q.M., Wang, S.: *Phys. Plasmas* **13**, 012309 (2006)
- Fu, H.S., Khotyaintsev, Y.V., André, M., Vaivads, A.: *Geophys. Res. Lett.* **38**, L16104 (2011)
- Fu, H.S., Cao, J.B., Khotyaintsev, Y.V., Sitnov, M.I., Runov, A., Fu, S.Y., Hamrin, M., André, M., Retinò, A., Ma, Y.D., Lu, H.Y., Wei, X.H., Huang, S.Y.: *Geophys. Res. Lett.* **40**, 6023 (2013)
- Guo, F., Li, H., Daughton, W., Liu, Y.H.: *Phys. Rev. Lett.* **113**, 155005 (2014)
- Guo, Z.F., Lin, Y., Wang, X.Y., Du, A.M.: *J. Geophys. Res.* **123**, 9169 (2018)
- Holman, G.D., Sui, L.H., Schwartz, R.A., Emslie, A.G.: *Astrophys. J.* **595**, L97 (2003)
- Hoshino, M., Mukai, T., Terasawa, T., Shinohara, I.: *J. Geophys. Res.* **106**, 25979 (2001)
- Huang, C., Lu, Q.M., Wang, S.: *Phys. Plasmas* **17**, 072306 (2010)
- Huang, S.Y., Vaivads, A., Khotyaintsev, Y.V., Zhou, M., Fu, H.S., Retinò, A., Deng, X.H., André, M., Cully, C.M., He, J.S., Sahrouri, F., Yuan, Z.G., Pang, Y.: *Geophys. Res. Lett.* **39**, L11103 (2012)
- Huang, C., Lu, Q.M., Wang, P.R., Wu, M.Y., Wang, S.: *J. Geophys. Res.* **119**, 6445 (2014)
- Huang, C., Lu, Q.M., Wang, R.S., Guo, F., Wu, M.Y., Lu, S., Wang, S.: *Astrophys. J.* **835**, 245 (2017)
- Imada, S., Nakamura, R., Daly, P.W., Hoshino, M., Baumjohann, W., Mühlbacher, S., Balogh, A., Rème, H.: *J. Geophys. Res.* **112**, A03202 (2007)
- Krucker, S., Hudson, H.S., Glesener, L., White, S.M., Masuda, S., Wuelsel, J.P., Lin, R.P.: *Astrophys. J.* **714**, 1108 (2010)
- Li, X.C., Guo, F., Li, H., Li, G.: *Astrophys. J.* **843**, 21 (2017)
- Lu, S., Lu, Q.M., Huang, C., Dong, Q.L., Zhu, J.Q., Sheng, Z.M., Wang, S., Zhang, J.: *New J. Phys.* **16**, 083021 (2014)
- Lu, S., Lu, Q.M., Lin, Y., Wang, X.Y., Ge, Y.S., Wang, R.S., Zhou, M., Fu, H.S., Huang, C., Wu, M.Y., Wang, S.: *J. Geophys. Res.* **120**, 6286 (2015)
- Lu, S., Angelopoulos, V., Fu, H.S.: *J. Geophys. Res.* **121**, 9483 (2016)
- Lu, Q.M., Wang, H.Y., Huang, K., Wang, R.S., Wang, S.: *Phys. Plasmas* **25**, 072126 (2018)
- Ma, Z.W., Wang, L.C., Li, L.J.: *Phys. Plasmas* **22**, 062104 (2015)
- Miller, J.A., Cargill, P.J., Emslie, A.G., Holman, G.D., Dennis, B.R., Larosa, T.N., Winglee, R.M., Benka, S.G., Tsuneta, S.: *J. Geophys. Res.* **102**, 14631 (1997)
- Nakamura, T.K.M., Fujimoto, M.: *Phys. Rev. Lett.* **101**, 165002 (2008)
- Northrop, T.G.: *Rev. Geophys.* **1**, 283 (1963)
- Øieroset, M., Lin, R.P., Phan, T.D., Larson, D.E., Bale, S.D.: *Phys. Rev. Lett.* **89**, 195001 (2002)
- Oka, M., Phan, T.D., Krucker, S., Fujimoto, M., Shinohara, I.: *Astrophys. J.* **714**, 915 (2010)
- Oka, M., Krucker, S., Hudson, H.S., Saint-Hilaire, P.: *Astrophys. J.* **799**, 129 (2015)
- Pritchett, P.L.: *Phys. Plasmas* **14**, 052102 (2007)
- Pritchett, P.L.: *Phys. Plasmas* **15**, 102105 (2008)
- Shibata, K., Takasao, S.: In: Gonzalez, W., Parker, E. (eds.) *Magnetic Reconnection*. *Astrophys. Space Sci. Library* (2016). https://doi.org/10.1007/978-3-319-26432-5_10
- Shibata, K., Tanuma, T.: *Earth Planets Space* **53**, 473 (2001)
- Shibata, K., Masuda, S., Shimojo, M., Hara, H., Yokoyama, T., Tsuneta, S., Kosugi, T., Ogawara, Y.: *Astrophys. J.* **451**, L83 (1995)

- Wang, R.S., Lu, Q.M., Du, A.M., Wang, S.: *Phys. Rev. Lett.* **104**, 175003 (2010)
- Wang, R.S., Lu, Q.M., Khotyaintsev, Y.V., Volwerk, M., Du, A.M., Nakamura, R., Gonzalez, W.D., Sun, X., Baumjohann, W., Li, X., Zhang, T.L., Fazakerley, A.N., Huang, C., Wu, M.Y.: *Geophys. Res. Lett.* **41**, 4851 (2014)
- Wang, H.Y., Lu, Q.M., Huang, C., Wang, S.: *Astrophys. J.* **821**, 84 (2016)
- Wang, R.S., Lu, Q.M., Nakamura, R., Huang, C., Du, A.M., Guo, F., Teh, W.L., Wu, M.Y., Lu, S., Wang, S.: *Nat. Phys.* **12**, 263 (2016)
- Wang, H.Y., Lu, Q.M., Huang, C., Wang, S.: *Phys. Plasmas* **24**, 052113 (2017)
- Wu, M.Y., Lu, Q.M., Volwerk, M., Vörös, Z., Zhang, T.L., Shan, L.C., Huang, C.: *J. Geophys. Res.* **118**, 4804 (2013)
- Wu, M.Y., Huang, C., Lu, Q.M., Volwerk, M., Nakamura, R., Vörös, Z., Zhang, T.L., Wang, S.: *J. Geophys. Res.* **120**, 6320 (2015)
- Zank, G.P., Le Roux, J.A., Webb, G.M., Dosch, A., Khabarova, O.: *Astrophys. J.* **798**, 28 (2014)
- Zhao, Y., Wang, R.S., Lu, Q.M., Du, A.M., Yao, Z.H., Wu, M.Y.: *J. Geophys. Res.* **121**, 10898 (2016)
- Zhou, M., Berchem, J., Walker, R.J., El-Alaoui, M., Deng, X., Cazzola, E., Lapenta, G., Goldstein, M.T., Paterson, W.R., Pang, Y., Ergun, R.E., Lavraud, B., Liang, H., Russell, C.T., Strangeway, R.J., Zhao, C., Giles, B.L., Pollock, C.J., Lindqvist, P.A., Marklund, G., Wilder, F.D., Khotyaintsev, Y.V., Torbert, R.B., Burch, J.L.: *Phys. Rev. Lett.* **119**, 055101 (2017)
- Zhou, M., El-Alaoui, M., Lapenta, G., Berchem, J., Richard, R.L., Schriver, D., Walker, R.J.: *J. Geophys. Res.* **123**, 8087 (2018)